Geophysical Research Letters

RESEARCH LETTER
10.1029/2022GL101700

Explaining Forcing Efficacy With Pattern Effect and State Dependence

C. Zhou[1,2], M. Wang[1,2], M. D. Zelinka[3], Y. Liu[1,2], Y. Dong[4], and K. C. Armour[5]

[1]School of Atmospheric Sciences, Nanjing University, Nanjing, China, [2]Joint International Research Laboratory of Atmospheric and Earth System Sciences & Institute for Climate and Global Change Research, Nanjing University, Nanjing, China, [3]Lawrence Livermore National Laboratory, Livermore, CA, USA, [4]Lamont-Doherty Earth Observatory, Columbia University, Palisades, NY, USA, [5]School of Oceanography and Department of Atmospheric Sciences, University of Washington, Seattle, WA, USA

Key Points:

- Forcing efficacy can be explained with a combination of pattern effect and state dependence of feedbacks
- Efficacy is lower when there is relatively stronger forcing over the tropical western Pacific Ocean
- Efficacy is higher when the forcing is more positive, inducing less-stabilizing feedbacks at higher warming

Supporting Information:

Supporting Information may be found in the online version of this article.

Correspondence to:

C. Zhou,
czhou17@nju.edu.cn

Citation:

Zhou, C., Wang, M., Zelinka, M. D., Liu, Y., Dong, Y., & Armour, K. C. (2023). Explaining forcing efficacy with pattern effect and state dependence. *Geophysical Research Letters*, *50*, e2022GL101700. https://doi.org/10.1029/2022GL101700

Received 13 OCT 2022
Accepted 22 JAN 2023

Abstract The magnitude of global surface temperature change in response to unit radiative forcing depends on the type and magnitude of forcing agent—a concept known as a "forcing efficacy." However, the mechanisms behind the forcing efficacy are still unclear. In this study, we perform a set of simulations using CESM1 to calculate the efficacy of 10 different forcing agents defined in terms of fixed-SST effective radiative forcing, and then use a Green's function approach to show that each forcing efficacy can be largely understood in terms of the radiative feedbacks associated with the different surface temperature patterns induced by the forcing agents (a pattern effect). We also quantify how the state dependence of feedbacks on global mean surface temperature anomalies impacts forcing efficacies. The results show that the forcing efficacy can be well reconstructed with a combination of pattern effect and state dependence.

Plain Language Summary The magnitude of global warming in response to unit forcing induced by carbon dioxide is different to that induced by methane or solar radiation, and the efficacy of a specific climate forcing agent depends on its type and magnitude. Our results show that the forcing efficacy can be explained with a combination of pattern effect and state dependence. When there is relatively stronger forcing over the tropical western Pacific Ocean, where feedbacks are more negative, the corresponding sea surface warming pattern favors a lower efficacy. When the forcing induces a larger global surface warming, less-stabilizing feedbacks are induced and the corresponding efficacy tends to be higher.

1. Introduction

The climate system does not respond in the same way to CO_2 changes as it does to non-CO_2 forcing agents such as aerosols, methane or changes in incident solar radiation. The magnitude of global warming in response to unit radiative forcing depends on the type and magnitude of forcing agent applied (Hansen et al., 2005). The efficacy of a specific forcing agent can be defined as (Richardson et al., 2019)

$$E_{\mathrm{f}} = \frac{\Delta T / F}{\Delta T_{2\times \mathrm{CO}_2} / F_{2\times \mathrm{CO}_2}}, \tag{1}$$

where F is the magnitude of global mean radiative forcing, ΔT is the change of global mean surface temperature in response to the forcing, and $\Delta T_{2\times \mathrm{CO}_2}$ is the global mean surface temperature change in response to the forcing of a doubling of CO_2 ($F_{2\times \mathrm{CO}_2}$). Ideally, ΔT and $\Delta T_{2\times \mathrm{CO}_2}$ are defined as changes in equilibrium temperature, but in practice they are usually calculated as the temperature change averaged over a certain period of time after the forcing is applied. The radiative forcing used to calculate efficacy can be defined as either instantaneous radiative forcing or effective radiative forcing at top-of-atmosphere (TOA) or tropopause, and the efficacy has different values when different definitions are used. The efficacy defined with instantaneous radiative forcing is determined by both rapid radiative adjustment and radiative feedbacks, and the efficacy defined with effective radiative forcing is only affected by radiative feedback processes. Therefore the efficacy defined using effective radiative forcing is closer to unity than that defined with instantaneous radiative forcing (Richardson et al., 2019). Furthermore, the effective radiative forcing framework provides better understanding of the energy budget response to different drivers than the instantaneous radiative forcing framework (Hansen et al., 2005; Richardson et al., 2019; Sherwood et al., 2015), so efficacies are usually calculated under the effective radiative forcing framework in recent studies. The effective radiative forc-

ing can be defined relative to a fixed sea surface temperature (SST) scenario, or be calculated using linear regression. P. M. Forster et al. (2016) suggest that fixed-SST effective radiative forcing has more certainty than regression-based methods, and the fixed-SST method is recommended for diagnosing effective radiative forcing.

The efficacy can also be defined in terms of the ratio of the radiative feedback operating at equilibrium under a given forcing agent to the radiative feedback operating at equilibrium under CO_2 doubling (e.g., Richardson et al., 2019; Rose et al., 2014). Using the traditional global energy balance model (Gregory et al., 2004), we have

$$N = F - \lambda \Delta T, \tag{2}$$

where λ is the equilibrium climate feedback parameter in response to the forcing agent (defined as the absolute value of total net feedback in this study), and N is the anomalous TOA net flux. When the climate system reaches equilibrium, we have

$$\Delta T_{\mathrm{eq}} = \frac{F}{\lambda}, \tag{3}$$

where ΔT_{eq} is the global mean surface temperature change at equilibrium. Particularly, in response to a CO_2 doubling, we have

$$\Delta T_{\mathrm{eq},2\times CO_2} = \frac{F_{2\times CO_2}}{\lambda_{2\times CO_2}}, \tag{4}$$

where $\lambda_{2\times CO_2}$ is the climate feedback parameter for a doubling of CO_2. Combining Equations 1, 3 and 4, we have (Richardson et al., 2019; Rose et al., 2014)

$$E_{f,\lambda} = \frac{\lambda_{2\times CO_2}}{\lambda}. \tag{5}$$

When ΔT and $\Delta T_{2\times CO_2}$ in Equation 1 are defined as changes in equilibrium temperature, the efficacy defined using Equation 5 is equal to that defined using Equation 1. However, if ΔT and $\Delta T_{2\times CO_2}$ in Equation 1 are transient temperature changes, then the efficacy calculated using Equations 1 and 5 could be different.

Forcing efficacies have been proposed to arise from different forcing agents having different spatial patterns of forcing than CO_2 forcing (e.g., Hansen et al., 2005; Kummer & Dessler, 2014; Marvel et al., 2016; Rose et al., 2014; Shindell, 2014; Winton et al., 2010). When forcing is applied in regions of less-negative radiative feedbacks (a weaker radiative response per degree of warming), we can expect a larger warming per unit change of forcing, and thus an efficacy higher than 1 (e.g., Armour et al., 2013). This can be described as different forcing agents producing different global radiative feedbacks through the pattern of SST change they induce (Haugstad et al., 2017)—a "pattern effect." It is also possible that different radiative forcing agents produce different efficacies because they affect radiation at different heights in the atmosphere (Richardson et al., 2019).

On the other hand, radiative feedbacks can also depend on the magnitude of temperature change itself (a state dependence or feedback nonlinearity, Bloch-Johnson et al., 2021; Caballeroa & Huberb, 2013; Meraner et al., 2013). State dependence has been used in the refined model of Ceppi and Gregory (2019) to quantitatively explain the dependence of climate feedbacks on forcing agent, so it is possible that forcing efficacies may also depend on the magnitudes of radiative forcing through the magnitude of global temperature change they induce.

In this study, we first test the hypothesis (Haugstad et al., 2017) that the efficacy of a radiative forcing agent depends only on the surface temperature pattern it induces relative to that of CO_2 forcing, via the influence of that temperature pattern on radiative feedbacks. In this view, the vertical structure of the forcing plays no role except through its influence on the pattern of surface temperature change. We carry out a set of idealized experiments to determine the forcing efficacy and feedback state dependence, and apply a Green's function approach (GFA, Dong et al., 2019; Zhang et al., 2022; Zhou et al., 2017) to quantify the pattern effect. We further explore whether feedback nonlinearities with global temperature could play a role in the calculation of forcing efficacy, and establish a quantitative relationship between the radiative forcing efficacy and the combination of the pattern effect and state dependence of radiative feedbacks.

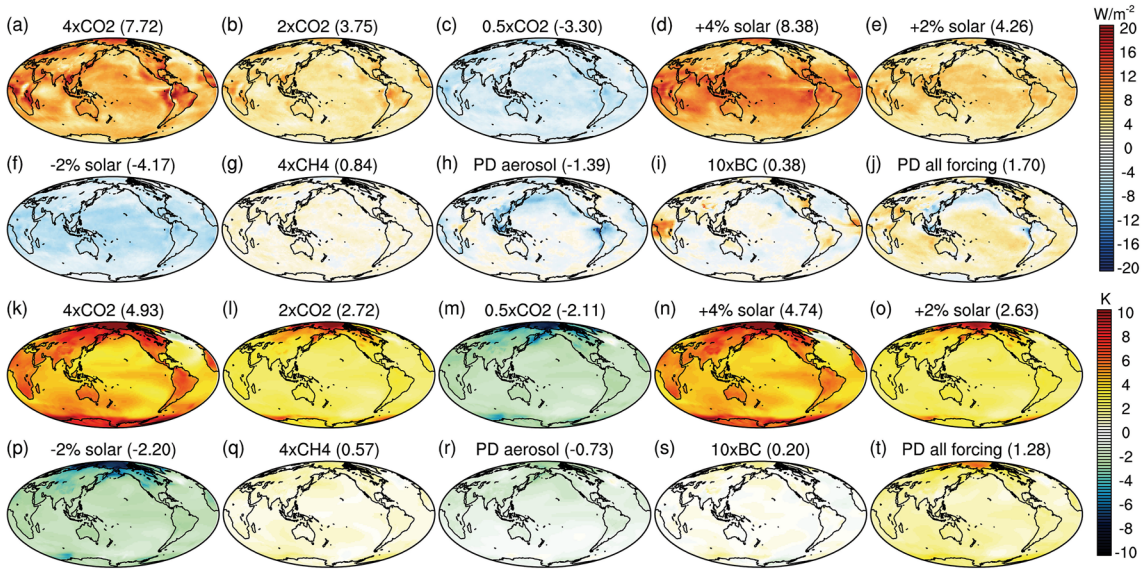

Figure 1. Spatial distribution of effective radiative forcing and surface temperature change. (a–j) Effective radiative forcing derived from the fixed-sea surface temperature experiments. (k–t) Surface temperature change in the abrupt forcing experiments, calculated as the change of surface temperature averaged over years 131–150 compared to the climatological mean values of the PI-control experiment. Numbers in the brackets denote global mean values.

2. Methods and Experiment Design

The simulations are performed using the Community Earth System Model 1.2.1 with Community Atmosphere Model 5.3 (CESM1.2.1-CAM5.3) at 1.9 latitude × 2.5 longitude resolution (Neale et al., 2012). The version of model used in this study is same as that used in Zhou et al. (2020), so that the patch experiments in Zhou et al. (2020) can be used to quantify the pattern effect using GFA.

We first perform a set of atmosphere-only experiments with fixed SST and sea ice cover (SIC) to calculate the effective radiative forcing, including one control run (where all radiative forcings are fixed at preindustrial levels) and 10 forcing experiments each with an abruptly changed radiative forcing agent (Table S1 in Supporting Information S1). To account for the effect of feedback state dependence, three levels of CO_2 and solar forcings are chosen in the experiments. Considering that there are many types of aerosols and greenhouse gases in the atmosphere, we performed a set of present day (PD) aerosol forcing experiments and a set of PD all forcing experiments to understand the overall efficacy of multiple forcing components.

To avoid assumptions in calculating the effect of land surface temperature change on the TOA energy balance (Hansen et al., 2005; Richardson et al., 2019), the fixed-SST effective radiative forcing is chosen to calculate the effective radiative forcing (Richardson et al., 2019):

$$F_i = N_{i,\mathrm{a}} - N_{0,\mathrm{a}}, \tag{6}$$

where $N_{0,\mathrm{a}}$ is the mean TOA radiative flux in the Fixed-SST control experiment, $N_{i,\mathrm{a}}$ is the mean TOA radiative flux in the ith forced experiment, and F_i is the effective radiative forcing of the corresponding forcing agent. Note that if the land surface temperature adjusted effective radiative forcing (Andrews et al., 2021; Hansen et al., 2005; Richardson et al., 2019) is used instead of the effective radiative forcing defined by Equation 6, there are only minor changes in the results of this paper (Table S2 in Supporting Information S1). The spatial distribution of effective radiative forcing for each experiment is shown in Figures 1a–1j.

The rapid adjustment of global mean surface temperature to the radiative forcings, which will be used to calculate the effective feedback parameter later (Equation 9), can be calculated as

$$\Delta T_{i,\mathrm{ra}} = T_{i,\mathrm{a}} - T_{0,\mathrm{a}}, \tag{7}$$

where $T_{i,\mathrm{a}}$ and $T_{0,\mathrm{a}}$ are the mean global surface temperature in the fixed-SST forced and control experiments, respectively. Surface air temperature is used as the surface temperature in this study.

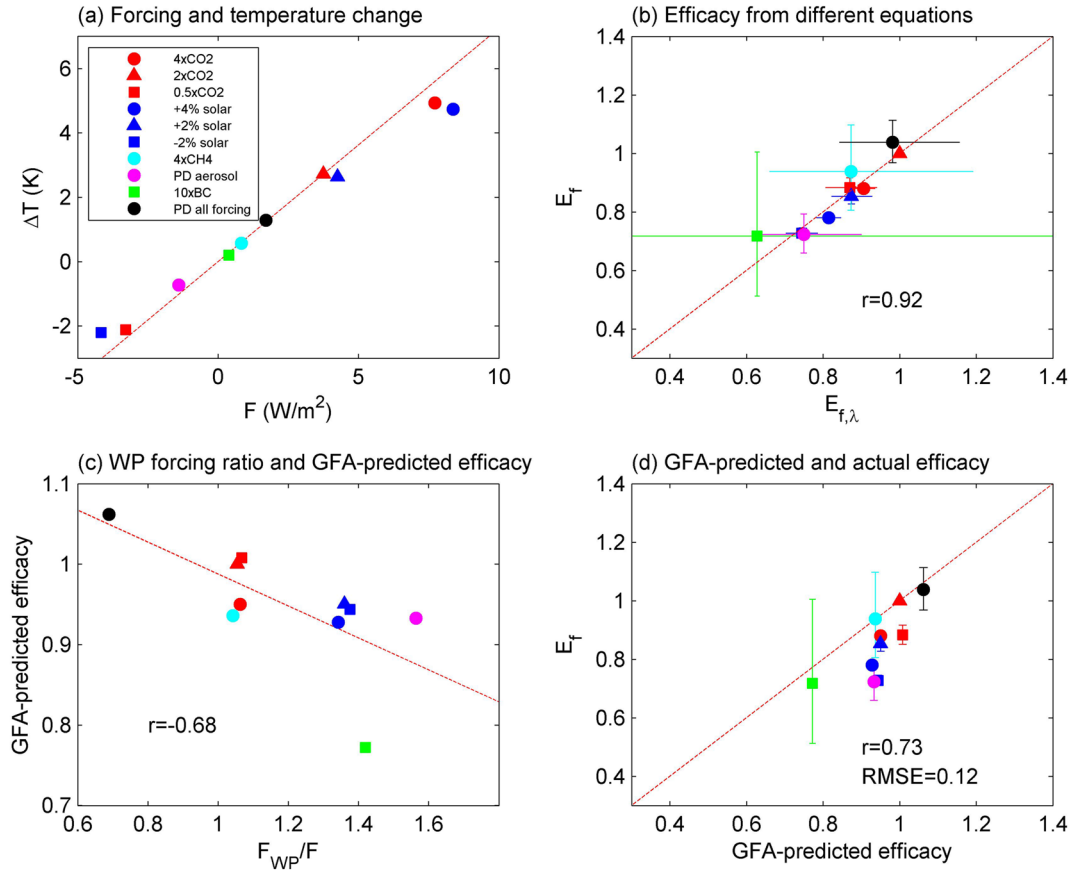

Figure 2. Contribution of pattern effect to variations in forcing efficacy. (a) Relationship between effective radiative forcing and surface temperature change. The red line indicates the relationship for an efficacy of 1, which passes through the $2 \times CO_2$ point with 0 intercept. (b) Relationship between efficacy calculated using Equations 1 and 5. (c) Relationship between F_{WP}/F (F_{WP} is the average effective radiative forcing in the Western Pacific Ocean, illustrated by the black rectangle of Figure 3a) and the Green's function approach (GFA)-reconstructed efficacy ($E_{f,GFA}$, Equation 13). The red line is a linear fit line. (d) Relationship between the GFA-reconstructed efficacy and actual efficacy (E_f, Equation 1). The red lines in (b, d) denote the $y = x$ lines. The error bars representing 5%–95% uncertainty intervals are calculated with bootstrapping, where 10,000 random sampling subsets are used to compute the statistical distribution of the efficacy for each case. Note that the uncertainty intervals of E_f are smaller than $E_{f,\lambda}$, so E_f is used in (d) instead of $E_{f,\lambda}$.

Subsequently, we perform a 250-year-long preindustrial control (PI-control) experiment with CESM1.2.1 (coupled ocean-atmosphere). Files for initial conditions are downloaded from the CESM official website, and the global mean surface temperature does not change significantly during the whole 250 years period, indicating that the climate system is at equilibrium. The last 150 years of the PI-control experiments are used to calculate the base surface temperature ($T_{0,c}$) and base TOA radiative fluxes ($N_{0,c}$).

Then 10 fully-coupled abrupt forcing experiments are branched from Year 100 of the PI-control experiment. In each of these 10 experiments, the radiative forcing is changed abruptly from the PI level to a new level, and held constant throughout the simulation. Each of these experiments are run for 150 years, and the last 20 years are used to calculate the new surface temperature ($T_{i,c}$, where i denote the ith forcer) and TOA radiative fluxes ($N_{i,c}$). The change of global mean surface temperature induced by the ith forcer can be calculated as

$$\Delta T_i = T_{i,c} - T_{0,c}. \tag{8}$$

The spatial distribution of temperature change is shown in Figures 1k–1t, and the relationship between global ΔT_i and F_i is shown in Figure 2a. Then the efficacy of ith forcer (E_f) can be calculated using Equation 1 or Equation 5 (Table S2 in Supporting Information S1). Though these abrupt forcing experiments do not reach equilibrium, global energy imbalance is relatively small toward the end of the runs, so we expect that the two efficacy definitions Equations 1 and 5 should produce similar results (Figure 2b).

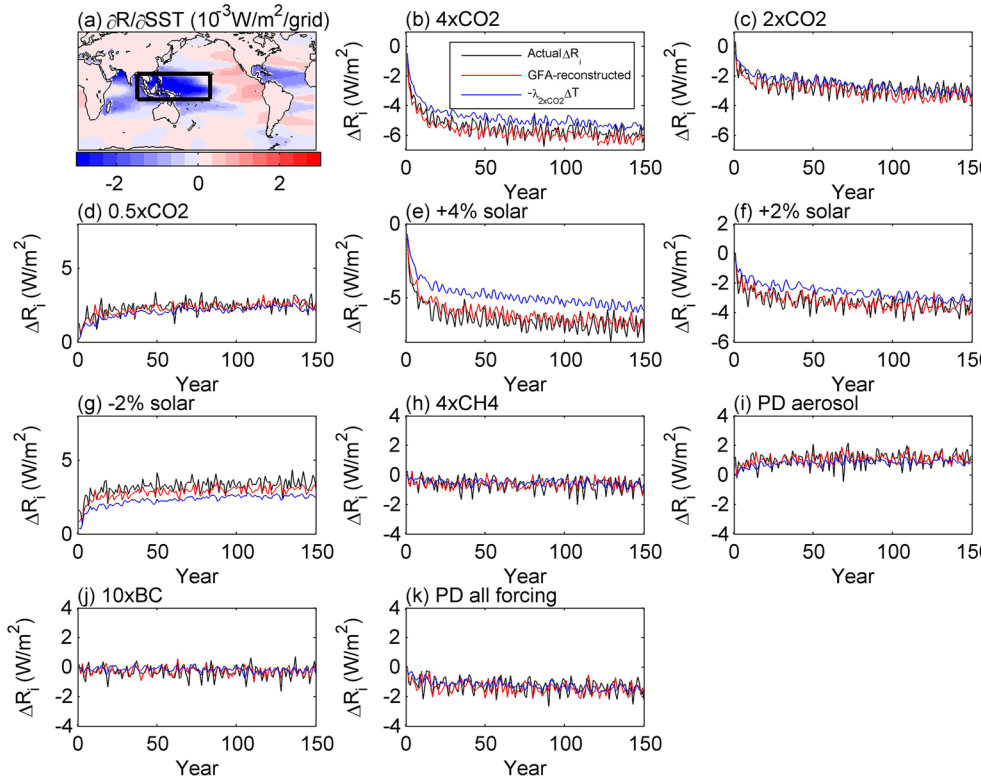

Figure 3. Reconstructing the feedback induced top-of-atmosphere (TOA) radiative flux anomalies (ΔR_i) using a Green's function approach (GFA). (a) Sensitivity of global TOA net flux to unit SST change in each grid box ($\partial R/\partial \mathrm{SST}_j$ of Equation 10). (b–k) Time series of ΔR_i in abrupt forcing experiments. Black lines denote actual ΔR_i calculated with Equation 11, red lines denote GFA-reconstructed values using Equation 10, and blue lines denote values reconstructed using a fixed feedback parameter $\lambda_{2\mathrm{xCO_2}}$.

To avoid climate feedback signals on the interannual timescale, regression is not used in this study, and we calculate the effective feedback parameter (Rugenstein & Armour, 2021) using the following equation,

$$\lambda_i = -\frac{\Delta R_i}{\Delta T_{i,\mathrm{fb}}} = -\frac{N_{i,\mathrm{c}} - N_{0,\mathrm{c}} - F_i}{\Delta T_i - \Delta T_{i,\mathrm{ra}}}, \tag{9}$$

where ΔR_i denotes the change of TOA radiative fluxes in response to feedback-induced global mean surface temperature changes ($\Delta T_{i,\mathrm{fb}}$, which equals to the difference between total temperature change and rapid adjustment induced temperature change). Then the feedback-derived efficacy can be calculated using Equation 5. (Table S2 in Supporting Information S1)

3. Contribution of the Pattern Effect to Forcing Efficacy

The pattern effect is analyzed using GFA (Dong et al., 2019; Zhang et al., 2022; Zhou et al., 2017). In particular, SST-induced TOA radiation anomalies can be quantified using

$$\Delta R_{i,\mathrm{GFA}} = \sum_j \frac{\partial R}{\partial \mathrm{SST}_j} \Delta \mathrm{SST}_j + \varepsilon, \tag{10}$$

where $\Delta \mathrm{SST}_j$ is the change of SST in a specific grid box j, calculated as the difference between the SST in the abrupt forcing experiment and the climatological mean SST in the PI-control experiment. $\partial R/\partial \mathrm{SST}_j$ is the sensitivity of global mean net TOA fluxes to SST change in the jth grid box (Figure 3a), and is calculated using the experiments of Zhou et al. (2020) (Figure S1 in Supporting Information S1). ε is an error term representing nonlinear effects that are not captured by the Green's function.

Figures 3b–3k show that the GFA-predicted TOA radiation feedback closely correspond with the actual values, which is calculated as

$$\Delta R_i = N_{i,c} - N_{0,c} - F_i, \tag{11}$$

indicating that GFA is effective in quantifying the pattern effect in these abrupt forcing experiments. Note that the performance of GFA for explaining the pattern effect might be different for other models (Dong et al., 2019; Zhang et al., 2022). The TOA radiation anomalies implied by a fixed climate feedback parameter are also shown in Figures 3b–3k, and the differences between the blue lines and black lines in Figure 3 are primarily induced by the pattern effect. Then the feedback parameter induced by pattern effect can be reconstructed as

$$\lambda_{i,\mathrm{GFA}} = -\frac{\Delta R_{i,\mathrm{GFA}}}{\Delta T_{i,\mathrm{fb}}} = -\frac{\sum_j \frac{\partial R}{\partial SST_j}\Delta SST_j}{\Delta T_i - \Delta T_{i,\mathrm{ra}}}, \tag{12}$$

and the efficacy of each forcing agent can be reconstructed using Equations 2 and 8,

$$E_{f,\mathrm{GFA}} = \frac{\lambda_{2\times CO_2,\mathrm{GFA}}}{\lambda_{i,\mathrm{GFA}}}, \tag{13}$$

The value of $\partial R/\partial \mathrm{SST}_j$ is strongly negative over the tropical western Pacific Ocean (the black box of Figure 3a, which is similar to but slightly different from the region chosen by Dong et al., 2019), so it is expected that stronger effective radiative forcing and SST warming over this region results in lower efficacy. To test this mechanism, we calculate the ratio of effective radiative forcing in the Western Pacific Ocean to the global effective radiative forcing (WP forcing ratio), and find that this ratio is negatively correlated with $E_{\mathrm{f,GFA}}$ (Figure 2c) and E_{f} ($r = -0.90$) as expected. Specifically, the GFA-reconstructed efficacy is greatest in the PD all forcing experiment, where the average forcing is weak in the tropical western Pacific Ocean compared to other regions (Figure 1). On the contrary, the GFA-reconstructed efficacy is smallest in the 10 × BC experiment, and the average forcing over the tropical western Pacific Ocean is strong compared to other regions in this experiment. It is worth noting that the efficacy of individual forcing components is lower than or equal to unity, but the efficacy of PD all forcing is slightly higher than unity. In the PD all forcing experiment, greenhouse gas induced warming is partially counteracted by the aerosol induced cooling. The efficacy of aerosol is less than that of greenhouse gases, so the aerosol induced temperature change is less negative compared to the case with an aerosol efficacy of unity, and as a result the overall efficacy of PD all forcing is higher than unity.

The forcing efficacies reconstructed by the GFA are well correlated with actual values (Figure 2d). Given that the GFA reconstruction is solely based on the SST patterns induced by the forcings without needing the forcing structures, this result indicates that the pattern effect is important in determining the forcing efficacies. Nevertheless, the GFA-predicted efficacies are systematically higher than actual values. In the following section, we examine whether this systematic overestimation might partially result from a neglect of feedback state dependence.

4. Explaining the Forcing Efficacy With a Combination of Pattern Effect and State Dependence

To quantify the state dependence of radiative feedbacks, we perform a set of uniform warming experiments (Table S1 in Supporting Information S1). In each uniform warming experiment, we apply a uniform warming or cooling everywhere over the global oceans, and fix all radiative forcing agents and SIC at preindustrial levels as in the Fixed-SST control experiment.

Figure 4a shows the relationship between TOA radiative fluxes changes (ΔR) and global mean surface temperature changes (ΔT) in these uniform warming experiments. ΔR decreases monotonically with ΔT, but at a rate that depends in subtle ways on ΔT, so the feedback parameter in response to uniform warming is a function of global mean surface temperature change,

$$\lambda_{\mathrm{uni}}(\Delta T) = -\frac{R_{\mathrm{uni}}(\Delta T) - R_{\mathrm{uni}}(0)}{\Delta T}, \tag{14}$$

where ΔT is the change of global mean surface temperature compared to the control experiment, and $R_{\mathrm{uni}}(\Delta T)$ is the mean TOA radiative fluxes in the uniform warming experiment. Based on the six simulations we performed (circles in Figure 4a), we further derive an empirical function of λ_{uni} (ΔT) using two interpolation methods, quadratic fit (e.g., Bloch-Johnson et al., 2021) and spline interpolation. The results suggest that the feedback

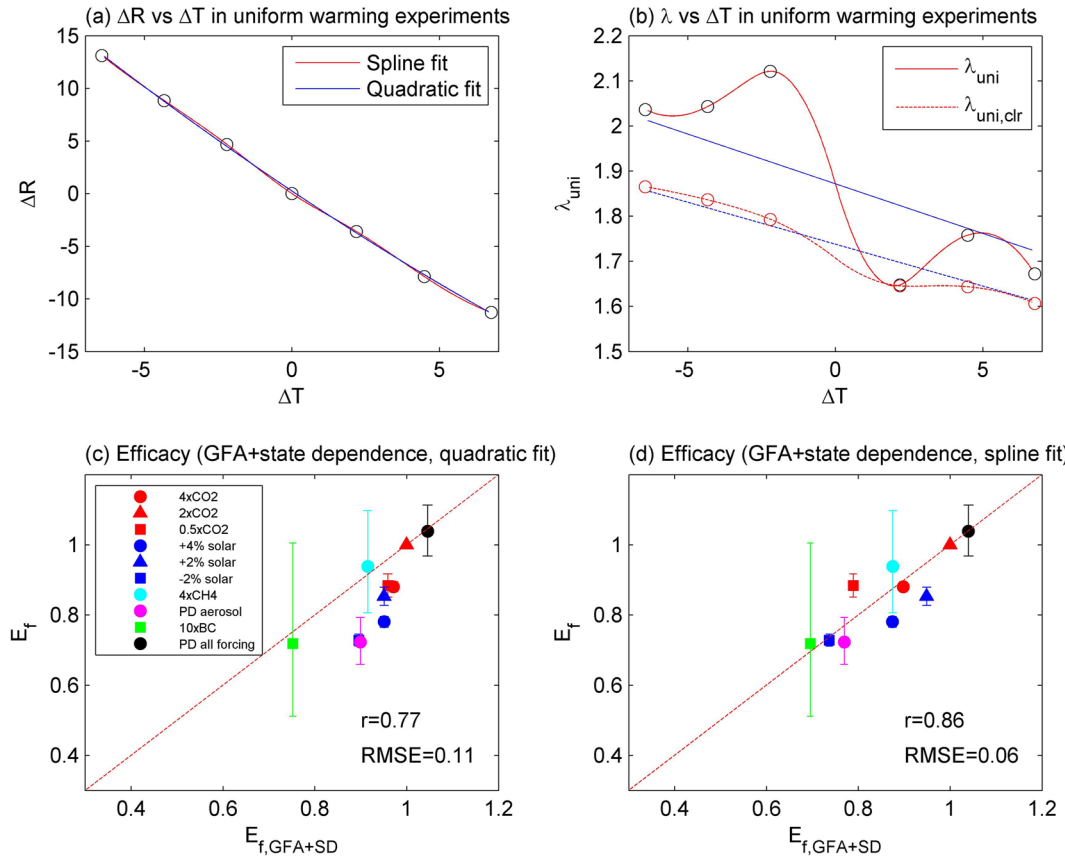

Figure 4. Reconstruction of efficacy with a combination of pattern effect and state dependence. (a) Relationship between ΔT and ΔR in uniform warming experiments. Black circles denote values calculated from the uniform warming experiments. The blue line is a quadratic fit line, and the red line is calculated using spline interpolation. (b) The state dependence of climate feedback parameter as a function of ΔT. Black circles denote allsky values calculated from the uniform warming experiments, and red circles denote clearsky values. The blue and red solid lines denote the feedback parameters calculated from the interpolated lines of (a), and the dashed lines denote clear-sky values calculated using the corresponding interpolation method. (c, d) Relationship between Green's function approach + state dependence reconstructed efficacy ($E_{\mathrm{f,GFA+SD}}$, Equation 16) and actual efficacy (E_{f}) calculated using quadratic and spline fits, respectively. The error bars in (c, d) denote 5%–95% uncertainty intervals, and are calculated with bootstrapping.

parameter generally decreases (higher efficacy) as temperature increases (Figure 4b), which is broadly consistent with the results and theories of previous studies (Bloch-Johnson et al., 2021; Caballeroa & Huberb, 2013; Kolla & Cronina, 2018; Meraner et al., 2013; Seeley & Jeevanjee, 2021). When quadratic fit is used in the calculation of λ_{uni}, λ_{uni} is a linear function, and the clearsky fluxes are the primary contributor to the change of λ_{uni}. When spline interpolation is applied, the value of λ_{uni} is no longer linear with ΔT, and cloud feedback becomes an important contributor to the state dependence in this case. Note that spline interpolation captures more nonlinear features than quadratic fit, but its results may be potentially affected by overfitting, so results from both methods are shown in this paper.

Then the contribution of feedback state dependence to forcing efficacy can be quantified using Equation 5 as

$$E_{\mathrm{f,SD}}(\Delta T_i) = \frac{\lambda_{\mathrm{uni}}\left(\Delta T_{2\times \mathrm{CO}_2}\right)}{\lambda_{\mathrm{uni}}(\Delta T_i)}. \tag{15}$$

Combining Equations 13 and 15, we can reconstruct the efficacy of each forcer with a combination of pattern effect and non-linearity, and the overall efficacy is computed as the product of $E_{\mathrm{f,GFA}}$ and $E_{\mathrm{f,SD}}$

$$E_{\mathrm{f,GFA+SD}} = \frac{\lambda_{\mathrm{uni}}\left(\Delta T_{2\times \mathrm{CO}_2}\right)}{\lambda_{\mathrm{uni}}(\Delta T_i)} E_{\mathrm{f,GFA}}. \tag{16}$$

Figures 4c and 4d show that the values of $E_{f,GFA+SD}$ better reproduce the actual efficacies, no matter which interpolation method is used. Therefore, we can conclude that the efficacy of climate forcers is determined by both pattern effect and the state dependence of radiative feedbacks.

5. Conclusions and Discussions

In this paper, a series of idealized simulations are designed to quantify the radiative forcing efficacy of 10 different forcing agents, where efficacy is defined relative to the fixed-SST effective radiative forcing. The efficacies reproduced with a combination of pattern effect and state dependence correspond closely with actual values, indicating that the efficacies are determined by feedback dependence on both the pattern of sea surface warming and the magnitude of global surface temperature change.

The contribution of pattern effect to forcing efficacy is calculated using the GFA—an approach effectively representing the TOA radiation response to a given SST pattern (Dong et al., 2019; Zhang et al., 2022; Zhou et al., 2017). When there is more warming over tropical ascent regions compared to the abrupt $2 \times CO_2$ experiment (which is usually associated with more positive radiative forcings in these regions, Figure 2c), there are more low clouds globally (Zhou et al., 2016, 2017), and the lapse rate is weaker (Ceppi & Gregory, 2017; Dong et al., 2019), leading to more negative TOA radiative fluxes, and the pattern-induced efficacy deviates from unity.

The contribution of feedback state dependence to forcing efficacy is quantified using a set of additional simulations with uniform surface warming. When the change in global surface temperature is negative (i.e., non-BC aerosol forcings, and reduced solar/CO_2 forcing), the overall radiative damping is stronger than that in the $2 \times CO_2$ experiment, and this state dependence reduces the efficacy.

It is worth noting that the results in this paper depend on the definition of efficacy. For example, efficacy would be affected by differences in rapid adjustments if efficacy were defined under the instantaneous radiative forcing framework.

This study is based on one climate model (CESM1.2.1), and pattern effect and state dependence for other climate models might be quantitatively different from this model. However, impacts of both pattern effects and state dependence on feedbacks have been identified in CMIP5 and CMIP6 models (Bloch-Johnson et al., 2021; Dong et al., 2020; P. Forster et al., 2021; Sherwood et al., 2020), so it is expected that pattern effect and state dependence are also important in determining the efficacy of other models.

Furthermore, the uncertainties on forcing efficacy are large, so it is usually difficult to accurately quantify the effect of efficacies on the Earth's energy budget in climate studies. Instead, we have shown here that it is more convenient to account for the effect of forcing efficacy by considering the effect of pattern effect and state dependence of radiative feedbacks.

Acknowledgments
CZ and YL's work was supported by the National Natural Science Foundation of China (Grants NSFC 41875095 and 42075127), Research Funds for the Frontiers Science Center for Critical Earth Material Cycling, Nanjing University, and the Fundamental Research Funds for the Central Universities (0207/14380189). MDZ's work was supported by the U.S. Department of Energy (DOE) Regional and Global Model Analysis program area and was performed under the auspices of the DOE by Lawrence Livermore National Laboratory under Contract DE-AC52-07NA27344. YD was supported by the NOAA Climate and Global Change Postdoctoral Fellowship Program, administered by UCAR's Cooperative Programs for the Advancement of Earth System Science (CPAESS) under award NA210AR4310383. KCA was supported by National Science Foundation Grant AGS-1752796 and National Oceanic and Atmospheric Administration MAPP Program Award NA20OAR4310391.

Data Availability Statement

The experiment results that are used in this study are available online at Zenodo: https://doi.org/10.5281/zenodo.7193943.

References

Andrews, T., Smith, C. J., Myhre, G., Forster, P. M., Chadwick, R., & Ackerley, D. (2021). Effective radiative forcing in a GCM with fixed surface temperatures. *Journal of Geophysical Research: Atmospheres*, *126*(4), e2020JD033880. https://doi.org/10.1029/2020JD033880

Armour, K. C., Bitz, C. M., & Roe, G. H. (2013). Time-varying climate sensitivity from regional feedbacks. *Journal of Climate*, *26*(13), 4518–4534. https://doi.org/10.1175/JCLI-D-12-00544.1

Bloch-Johnson, J., Rugenstein, M., Stolpe, M. B., Rohrschneider, T., Zheng, Y., & Gregory, J. M. (2021). Climate sensitivity increases under higher CO_2 levels due to feedback temperature dependence. *Geophysical Research Letters*, *48*(4), e2020GL089074. https://doi.org/10.1029/2020GL089074

Caballeroa, R., & Huberb, M. (2013). State-dependent climate sensitivity in past warm climates and its implications for future climate projections. *Proceedings of the National Academy of Sciences*, *110*(35), 14162–14167. https://doi.org/10.1073/pnas.1303365110

Ceppi, P., & Gregory, J. M. (2017). Relationship of tropospheric stability to climate sensitivity and Earth's observed radiation budget. *Proceedings of the National Academy of Sciences*, *114*(50), 13126–13131. https://doi.org/10.1073/pnas.171430811

Ceppi, P., & Gregory, J. M. (2019). A refined model for the Earth's global energy balance. *Climate Dynamics*, *53*(7), 4781–4797. https://doi.org/10.1073/pnas.1714308114

Dong, Y., Armour, K. C., Zelinka, M. D., Proistosescu, C., Battisti, D. S., Zhou, C., & Andrews, T. (2020). Intermodel spread in the pattern effect and its contribution to climate sensitivity in CMIP5 and CMIP6 models. *Journal of Climate*, *33*(18), 7755–7775. https://doi.org/10.1175/jcli-d-19-1011.1

Dong, Y., Proistosescu, C., Armour, K. C., & Battisti, D. S. (2019). Attributing historical and future evolution of radiative feedbacks to regional warming patterns using a Green's function approach: The preeminence of the western Pacific. *Journal of Climate*, *32*(17), 5471–5491. https://doi.org/10.1175/JCLI-D-18-0843.1

Forster, P., Storelvmo, T., Armour, K., Collins, W., Dufresne, J.-L., Frame, D., et al. (2021). The Earth's energy budget, climate feedbacks, and climate sensitivity. In V. Masson-Delmotte, P. Zhai, A. Pirani, S. L. Connors, C. Péan, S. Berger, et al. (Eds.), *Climate change 2021: The physical science basis. Contribution of working group I to the sixth assessment report of the intergovernmental panel on climate change* (pp. 923–1054). Cambridge University Press. https://doi.org/10.1017/9781009157896.009

Forster, P. M., Richardson, T., Maycock, A. C., Smith, C. J., Samset, B. H., Myhre, G., et al. (2016). Recommendations for diagnosing effective radiative forcing from climate models for CMIP6. *Journal of Geophysical Research: Atmospheres*, *121*(20), 12460–12475. https://doi.org/10.1002/2016JD025320

Gregory, J. M., Ingram, W. J., Palmer, M. A., Jones, G. S., Stott, P. A., Thorpe, R. B., et al. (2004). A new method for diagnosing radiative forcing and climate sensitivity. *Geophysical Research Letters*, *31*(3), L03205. https://doi.org/10.1029/2003GL018747

Hansen, J., Sato, M., Ruedy, R., Nazarenko, L., Lacis, A., Schmidt, G., et al. (2005). Efficacy of climate forcings. *Journal of Geophysical Research*, *110*(D18), D18104. https://doi.org/10.1029/2005JD005776

Haugstad, A. D., Armour, K. C., Battisti, D. S., & Rose, B. E. J. (2017). Relative roles of surface temperature and climate forcing patterns in the inconstancy of radiative feedbacks. *Geophysical Research Letters*, *44*(14), 7455–7463. https://doi.org/10.1002/2017GL074372

Kolla, D. D. B., & Cronina, T. W. (2018). Earth's outgoing longwave radiation linear due to H_2O greenhouse effect. *Proceedings of the National Academy of Sciences*, *115*(41), 10293–10298. https://doi.org/10.1073/pnas.1809868115

Kummer, J. R., & Dessler, A. E. (2014). The impact of forcing efficacy on the equilibrium climate sensitivity. *Geophysical Research Letters*, *41*(10), 3565–3568. https://doi.org/10.1002/2014GL060046

Marvel, K., Schmidt, G. A., Miller, R. L., & Nazarenko, L. S. (2016). Implications for climate sensitivity from the response to individual forcings. *Nature Climate Change*, *6*(4), 386–389. https://doi.org/10.1038/nclimate2888

Meraner, K., Mauritsen, T., & Voigt, A. (2013). Robust increase in equilibrium climate sensitivity under global warming. *Geophysical Research Letters*, *40*(22), 5944–5948. https://doi.org/10.1002/2013GL058118

Neale, R. B., Chen, C. C., Gettelman, A., Lauritzen, P. H., Park, S., Williamson, D. L., et al. (2012). *Description of the NCAR community atmosphere model (CAM 5.0), report NCAR/TN-4861STR*. National Center for Atmospheric Research.

Richardson, T. B., Forster, P. M., Smith, C. J., Maycock, A. C., Wood, T., Andrews, T., et al. (2019). Efficacy of climate forcings in PDRMIP models. *Journal of Geophysical Research: Atmospheres*, *124*(23), 12824–12844. https://doi.org/10.1029/2019JD030581

Rose, B. E. J., Armour, K. C., Battisti, D. S., Feldl, N., & Koll, D. D. B. (2014). The dependence of transient climate sensitivity and radiative feedbacks on the spatial pattern of ocean heat uptake. *Geophysical Research Letters*, *41*(3), 1071–1078. https://doi.org/10.1002/2013GL058955

Rugenstein, M. A. A., & Armour, K. C. (2021). Three flavors of radiative feedbacks and their implications for estimating equilibrium climate sensitivity. *Geophysical Research Letters*, *48*(15), e2021GL092983. https://doi.org/10.1029/2021GL092983

Seeley, J. T., & Jeevanjee, N. (2021). H2O windows and CO2 radiator fins: A clear-sky explanation for the peak in equilibrium climate sensitivity. *Geophysical Research Letters*, *48*(4), e2020GL089609. https://doi.org/10.1029/2020GL089609

Sherwood, S. C., Bony, S., Boucher, O., Bretherton, C., Forster, P. M., Gregory, J. M., & Stevens, B. (2015). Adjustments in the forcing feedback framework for understanding climate change. *Bulletin of the American Meteorological Society*, *96*(2), 217–228. https://doi.org/10.1175/BAMS-D-13-00167.1

Sherwood, S. C., Webb, M. J., Annan, J. D., Armour, K. C., Forster, P. M., Hargreaves, J. C., et al. (2020). An assessment of Earth's climate sensitivity using multiple lines of evidence. *Reviews of Geophysics*, *58*(4), e2019RG000678. https://doi.org/10.1029/2019RG000678

Shindell, D. T. (2014). Inhomogeneous forcing and transient climate sensitivity. *Nature Climate Chang*e, 4(4), 274–277. https://doi.org/10.1038/NCLIMATE2136

Winton, M., Takahashi, K., & Held, I. M. (2010). Importance of ocean heat uptake efficacy to transient climate change. *Journal of Climate*, *23*(9), 2333–2344. https://doi.org/10.1175/2009JCLI3139.1

Zhang, B., Zhao, M., & Tan, Z. (2022). Using a Green's function approach to diagnose the pattern effect in GFDL AM4 and CM4. *Journal of Climate*, *36*(4), 1105–1125. https://doi.org/10.1175/JCLI-D-22-0024.1

Zhou, C., Lu, J., Hu, Y., & Zelinka, M. D. (2020). Responses of the Hadley circulation to regional sea surface temperature changes. *Journal of Climate*, *33*(2), 429–441. https://doi.org/10.1175/JCLI-D-19-0315.1

Zhou, C., Zelinka, M. D., & Klein, S. A. (2016). Impact of decadal cloud variations on the Earth's energy budget. *Nature Geoscience*, *9*(12), 871–874. https://doi.org/10.1038/ngeo2828

Zhou, C., Zelinka, M. D., & Klein, S. A. (2017). Analyzing the dependence of global cloud feedback on the spatial pattern of sea surface temperature change with a Green's function approach. *Journal of Advances in Modeling Earth Systems*, *9*(5), 2174–2189. https://doi.org/10.1002/2017MS001096